Electronic supplementary materials *Mendeleev Commun.*, 2025, **35**, 569–572

Partial lead substitution as a tool to manage the light-induced recrystallization and photostability of mixed-cation lead halide perovskites

Marina I. Ustinova, Gennady V. Shilov, Denis V. Korchagin, Nadezhda N. Dremova, Pavel A. Troshin, Sergey M. Aldoshin and Lyubov A. Frolova

Content

Materials and methods

Materials

Glass slides (25x25 mm) used as substrates were purchased from Isolab GmbH. Anhydrous dimethylacetamide (DMAc), dimethyl sulfoxide (DMSO) and toluene were purchased from Sigma-Aldrich and used as received inside nitrogen glove boxes. Formamidinium iodide (FAI, purity 99.9%) was purchased from FOMaterials Ltd. The following anhydrous reagents were purchased from Sigma-Aldrich (USA): CsI, PbI_2, CaI_2, SrI_2, BaI_2, PtI_2, EuI_2, SnI_2, MnI_2, FeI_2, CoI_2, CuI, AgI, ZnI_2, HgI_2, CdI_2, and SbI_3 (purity 99.999%); YI_3, NdI_3, DyI_2, YbI_2, and LuI_3 (purity 99.9%); GeI_2 (purity 99.8%); MgI_2, BiI_3, and InI_3 (purity 99.998%); NiI_2, LaI_3, CeI_3, ErI_3, TbI_3, and GdI_3 (purity 99.99%)

Perovskite films characterization

The UV-Vis absorption spectra were obtained using an AvaSpec-2048-2 UV-VIS fiber spectrometer integrated inside a glove box. The X-ray diffraction (XRD) patterns were collected using an Aeris instrument (Malvern PANalytical B.V.) with the CuKα source. The SEM characterization of the absorber films was performed using Zeiss SUPRA 25 instrument with Oxford Instruments EDX (Energy Dispersive X-ray) detector.

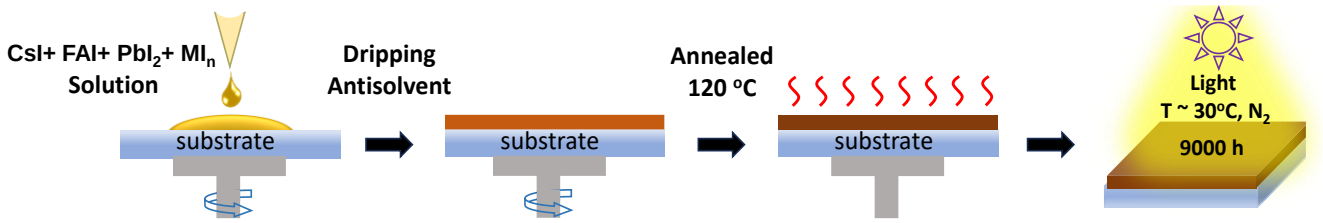

Figure S1 Schematic representation of the photochemical stability test.

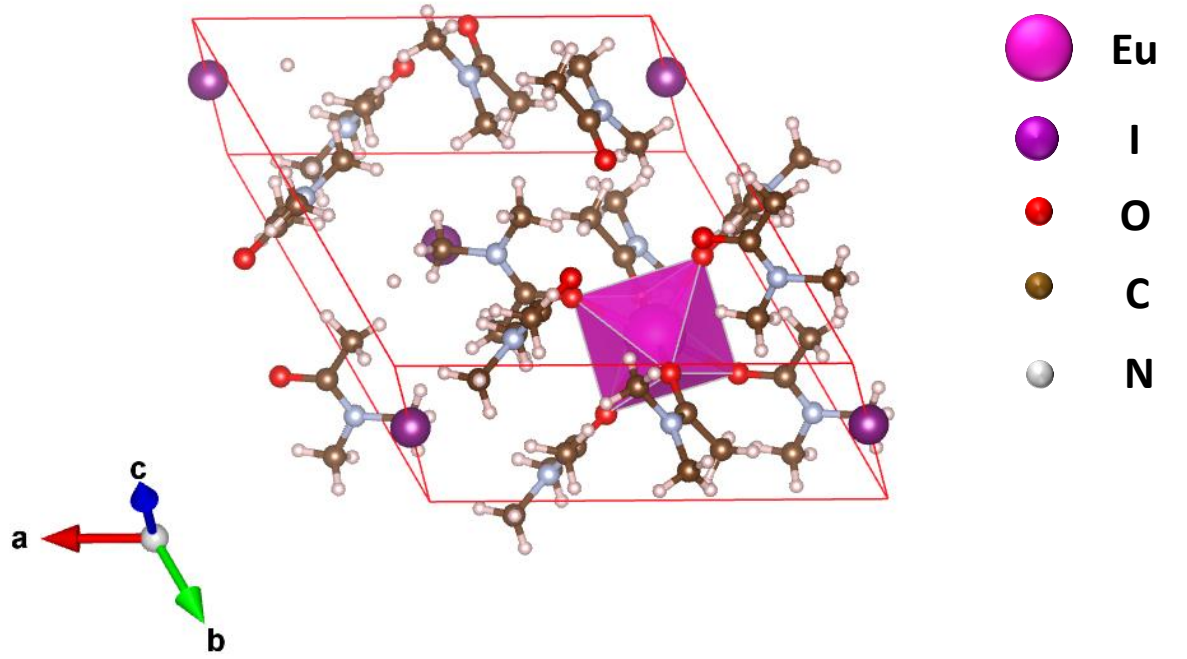

Figure S2. X-ray crystallography data for $Eu(DMAc)_2I_2$: 3D structure of the complex and crystal packing. Hydrogen atoms are omitted for clarity.

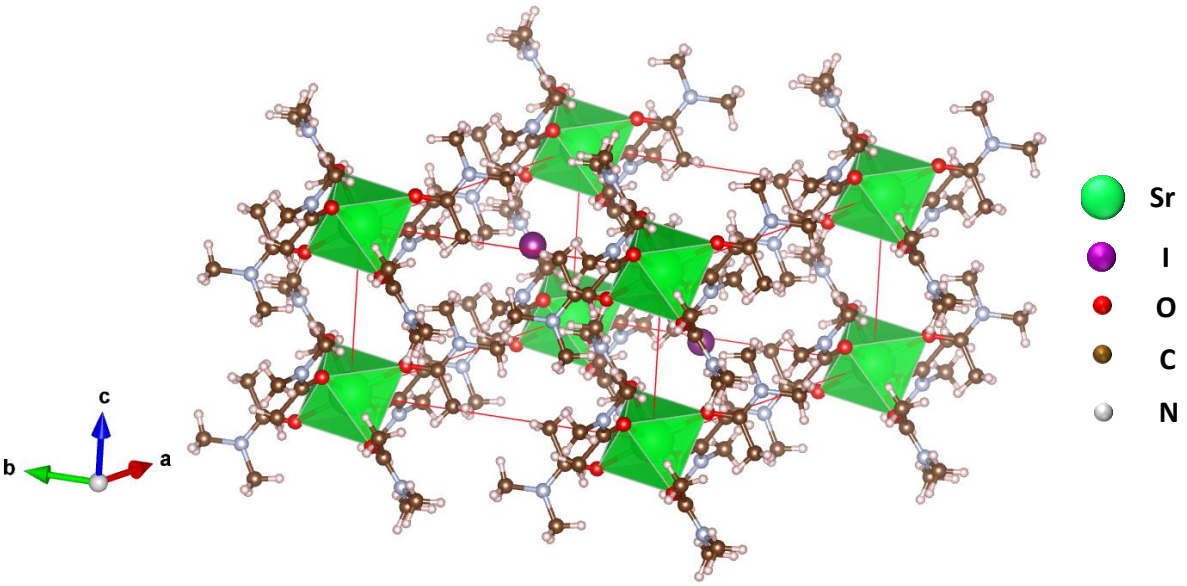

Figure S3. X-ray crystallography data for $Sr(DMAc)_6I_2$: 3D structure of the complex and crystal packing. Hydrogen atoms are omitted for clarity.

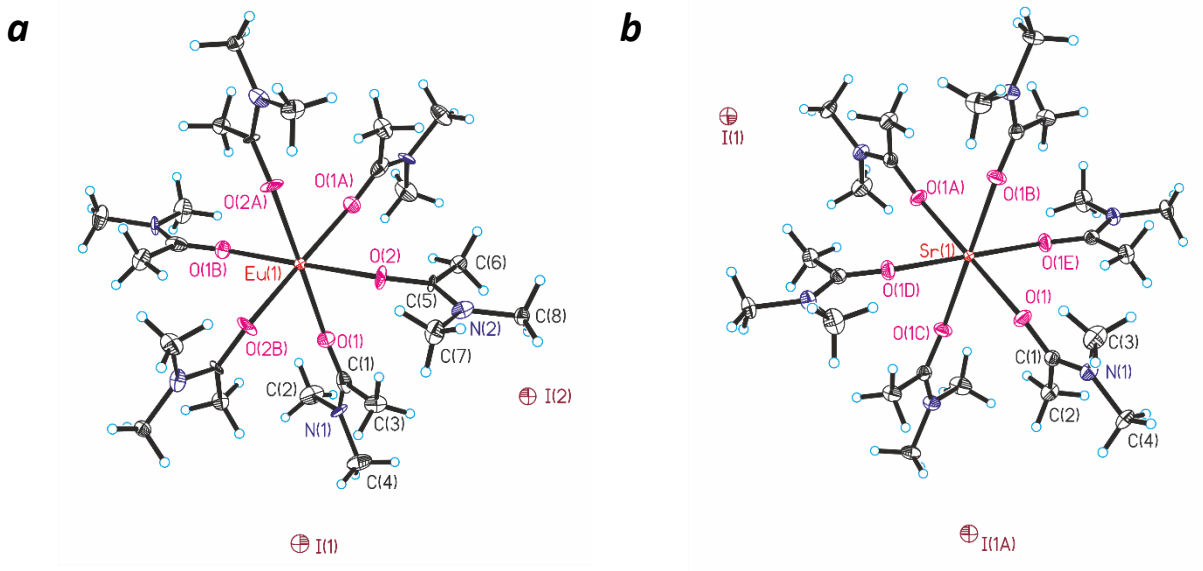

Figure S4. An ORTEP view of the $Eu(DMAc)_2I_2$ (a) and $Sr(DMAc)_2I_2$ (b) complexes (50% probability thermal ellipsoids).

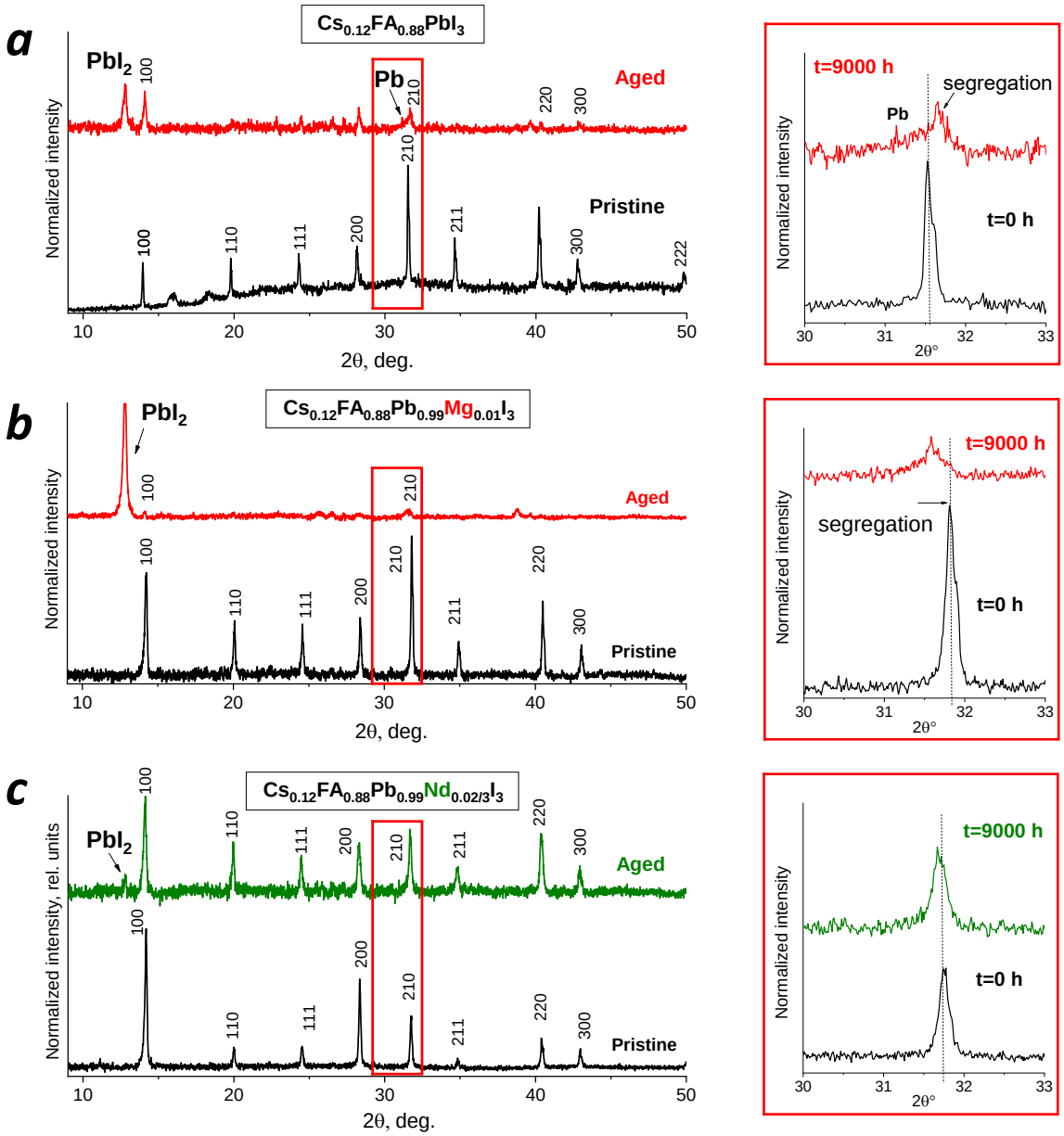

Figure S5. The XRD patterns of the representative perovskite films before and after 9000 h of continuous light soaking: reference non-modified $Cs_{0.12}FA_{0.88}PbI_3$ (a), $Cs_{0.12}FA_{0.88}Pb_{0.99}Mg_{0.01}I_3$ (b) and $Cs_{0.12}FA_{0.88}Pb_{0.99}Nd_{0.02/3}I_3$ (c).

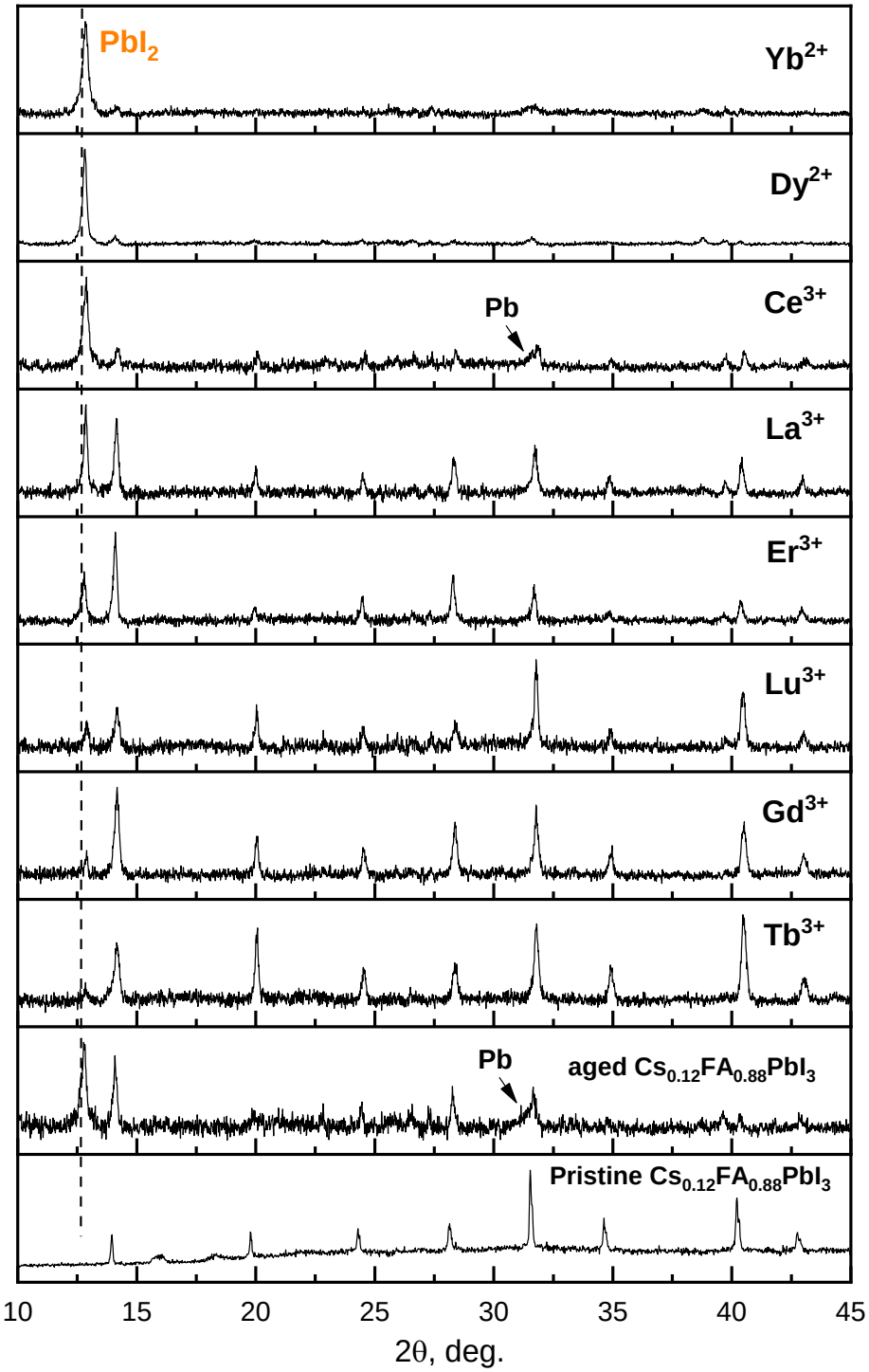

Figure S6. XRD patterns of the different $Cs_{0.12}FA_{0.88}Pb_{0.99}M_{(0.02/n)}I_3$ perovskite films after 9000 h of light exposure compared to the patterns of the pristine and aged $Cs_{0.12}FA_{0.88}PbI_3$ reference films.

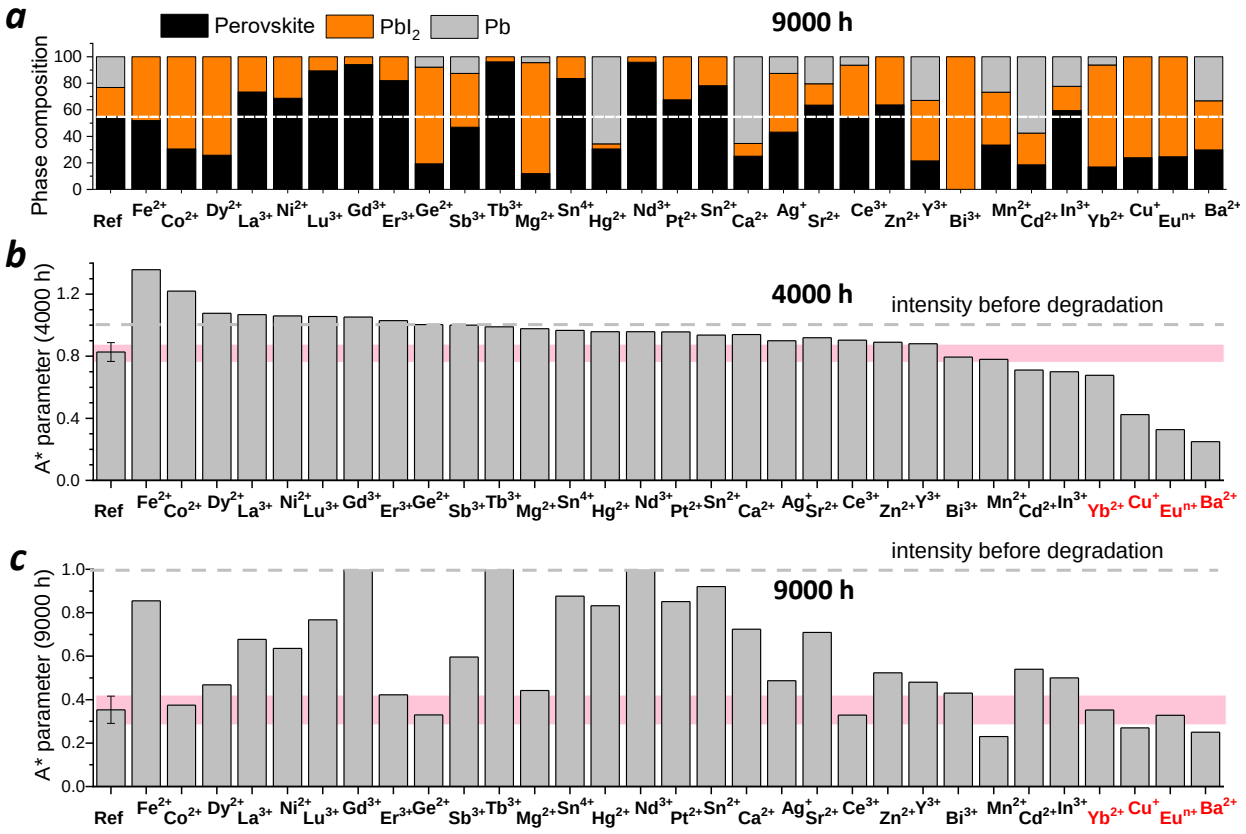

Figure S7. Overview of the photostability of different $Cs_{0.12}FA_{0.88}Pb_{0.99}M_{(0.02/n)}I_3$ materials formulations: the estimated phase composition of the films after 9000 h of light soaking (a) and the photobleaching of the perovskite films after 4000 h (b) and 9000 h (c) aging reflected by the A* parameter.

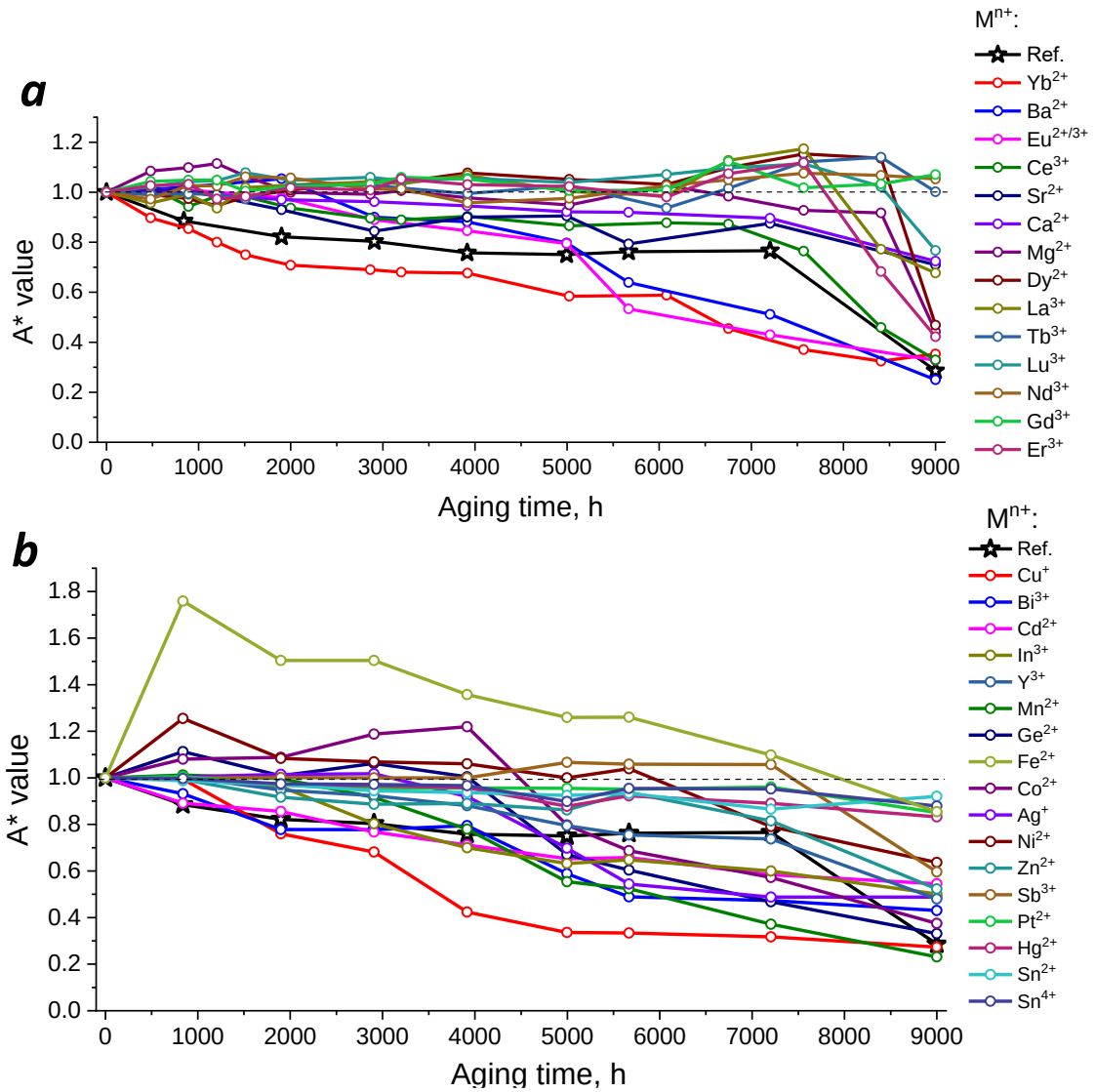

Figure S8. The dynamics of the photobleaching of the $Cs_{0.12}FA_{0.88}Pb_{0.99}M_{(0.02/n)}I_3$ perovskite films reflected by the evolution of A* parameter vs. aging time. Note that the A* values above 1.0 feature non-compensated light scattering effects induced by material recrystallization.

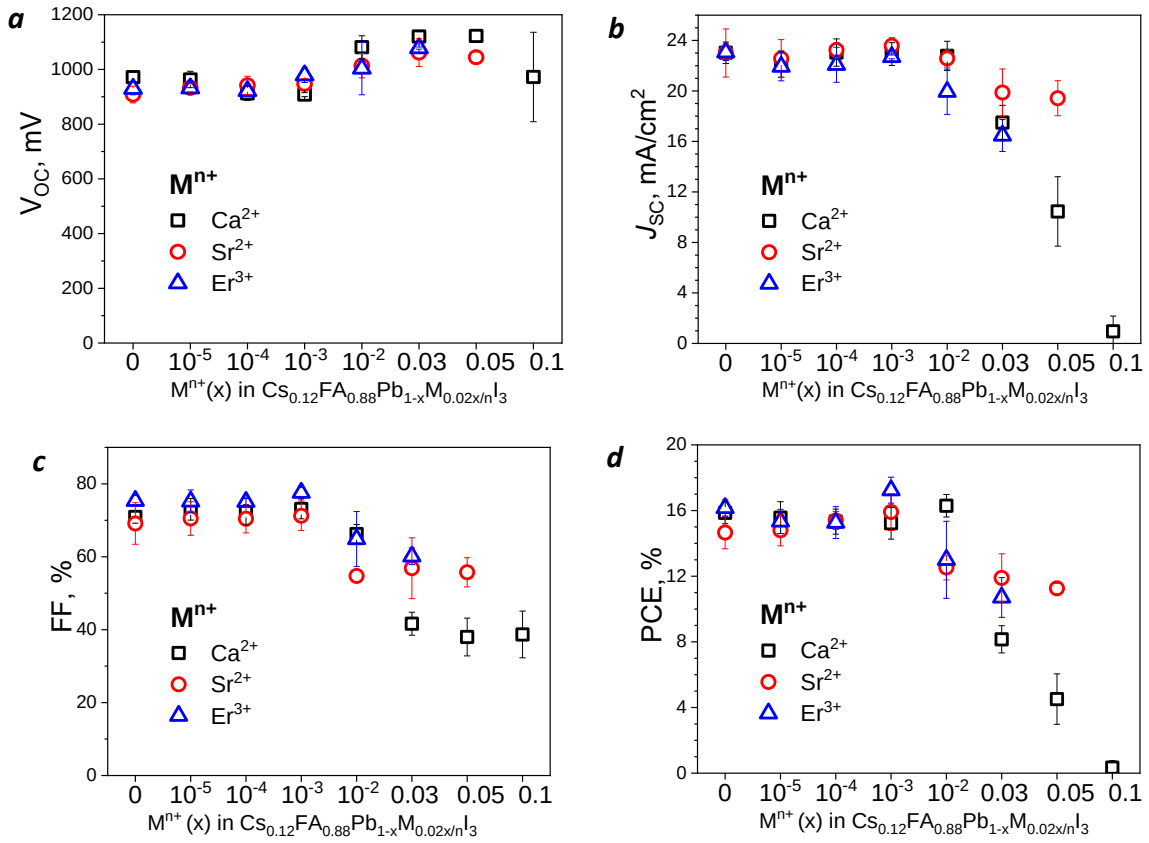

Figure S9. The optimization of PSCs performance by systematic variation of the x value (M^{n+} cation loading) in $Cs_{0.12}FA_{0.88}Pb_{1-x}M_{(0.02x/n)}I_3$ absorber films.

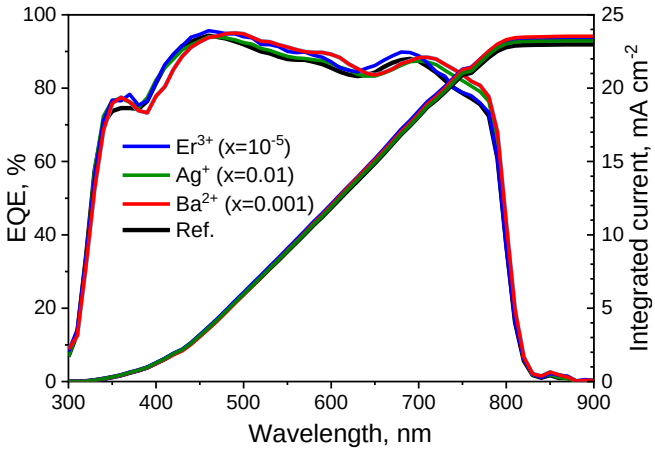

Figure S10. EQE spectra of the best-performing cells.

Table S1. The performance characteristics for the best $Cs_{0.12}FA_{0.88}Pb_{1-x}M_{(0.02x/n)}I_3$ absorber materials.*

M^{n+} (x value)	V_{OC}, mV	J_{SC}, mA/cm^2	FF, %	PCE, %
None (x=0)	950±8	23.9±0.2	73.0±0.2	16.6±0.4
Ba^{2+} ($x=10^{-5}$)	960±15	23.6±0.2	78.0±0.2	17.9±0.4
Ag^{+} (x=0.01)	997±19	23.2±0.2	76±0.2	17.6±0.5
Ca^{2+} (x=0.01)	1105±2	23.6±0.1	64.8±0.1	16.9±0.1
Sr^{2+} ($x=10^{-3}$)	975±2	22.9±0.3	74.8±0.6	16.9±0.1
Er^{3+} ($x=10^{-3}$)	985±17	23.6±0.2	78.1±0.2	17.6±0.5

* The characteristics were averaged for the forward and reverse scan J-V curves